Neutron inelastic scattering processes as a background for double-β decay experiments

D.-M. Mei,[1,2,*] S. R. Elliott,[1] A. Hime,[1] V. Gehman,[1,3] and K. Kazkaz[3,†]

[1]*Los Alamos National Laboratory, Los Alamos, New Mexico 87545, USA*

[2]*Department of Earth Science and Physics, University of South Dakota, Vermillion, South Dakota 57069, USA*

[3]*Center for Experimental Nuclear Physics and Astrophysics, and Department of Physics, University of Washington, Seattle, Washington 98195, USA*

(Received 3 April 2007; published 30 May 2008)

We investigate several Pb$(n, n'\gamma)$ and Ge$(n, n'\gamma)$ reactions. We measure γ-ray production from Pb$(n, n'\gamma)$ reactions that can be a significant background for double-β decay experiments which use lead as a massive inner shield. Particularly worrisome for Ge-based double-β decay experiments are the 2041-keV and 3062-keV γ rays produced via Pb$(n, n'\gamma)$. The former is very close to the ^{76}Ge double-β decay endpoint energy and the latter has a double escape peak energy near the endpoint. We discuss the implications of these γ rays on past and future double-β decay experiments and estimate the cross section to excite the level that produces the 3062-keV γ ray. Excitation γ-ray lines from Ge$(n, n'\gamma)$ reactions are also observed. We consider the contribution of such backgrounds and their impact on the sensitivity of next-generation searches for neutrinoless double-β decay using enriched germanium detectors.

DOI: 10.1103/PhysRevC.77.054614 PACS number(s): 23.40.−s, 25.40.Fq, 29.40.Wk

I. INTRODUCTION

Neutrinoless double-β decay plays a key role in understanding the neutrino's absolute mass scale and particle-antiparticle nature [1–4]. If this nuclear decay process exists, one would observe a monoenergetic line originating from a material containing an isotope subject to this decay mode. One such isotope that may undergo this decay is ^{76}Ge. Germanium-diode detectors fabricated from material enriched in ^{76}Ge have established the best half-life limits and the most restrictive constraints on the effective Majorana mass for the neutrino [5,6]. One analysis [7] of the data in Ref. [6] claims evidence for the decay with a half-life of 1.2×10^{25} yr. Planned Ge-based double-β decay experiments [8,9] will test this claim. Eventually, these future experiments will target a sensitivity of $>10^{27}$ yr or $\sim$1 event/ton yr to explore mass values near those indicated by the atmospheric neutrino oscillation results.

The key to these experiments lies in the ability to reduce intrinsic radioactive background to unprecedented levels and to adequately shield the detectors from external sources of radioactivity. Previous experiments' limiting backgrounds have been trace levels of natural decay chain isotopes within the detector and shielding components. The γ-ray emissions from these isotopes can deposit energy in the Ge detectors producing a continuum, which may overwhelm the potential neutrinoless double-β decay signal peak at 2039 keV. Great progress has been made identifying the location and origin of this contamination, and future efforts will substantially reduce this contribution to the background. The background level goal of 1 event/ton-year, however, is an ambitious factor of $\approx$400 improvement over the currently best achieved background level [6]. If the efforts to reduce the natural decay chain isotopes are to be successful, previously unimportant components of the background must be understood and eliminated. The potential for neutron reactions to be one of these background components is the focus of this paper. The work of Mei and Hime [10] recognized that $(n, n'\gamma)$ reactions will become important for ton-scale double-β decay experiments. Specifically, we have studied neutron reactions in Pb and Ge, materials that play important roles in the Majorana [8] design. But since lead is used by numerous low-background experiments, the results will have wider utility.

This paper presents measurements and simulations of Pb$(n, n'\gamma)$ and Ge$(n, n'\gamma)$ reactions and estimates the resulting background for Ge-detector-based, double-β decay experiments for a given neutron flux. With these results, we then use the neutron flux, energy spectrum, angular distribution, multiplicity, and lateral distributions determined in Ref. [10] to estimate the background in Ge detectors situated in underground laboratories. In Sec. II, we describe the experiments, data, and simulations. In Secs. III and IV, we describe the analysis of these data. Section IV also discusses the important Pb$(n, n'\gamma)$ production of γ rays at 2041 and 3062 keV. The former is dangerously near the 2039-keV Q value for zero-neutrino double-β decay in ^{76}Ge, and the latter can produce a double-escape peak line at 2040 keV. These dangerous processes for Ge-based double-β decay experiments are discussed for the first time in this work. Section V determines an overall background model for our detector and the implications of this model for future experimental designs. It also considers the relevant merits of Cu versus Pb as shielding materials and discusses the use of depth to mitigate these backgrounds. We also consider the possibility that the double-escape peak of the 3062-keV γ ray could contribute to the signal claimed in Ref. [7]. Finally, we summarize our conclusions in Sec. VI.

*Permanent address: Department of Earth Science and Physics, University of South Dakota, Vermillion, South Dakota 57069, USA.

†Permanent address: Lawrence Livermore National Laboratory, Livermore, California 94550, USA.

II. THE MEASUREMENTS

We collected five data sets to explore the implications of $(n, n'\gamma)$ for double-β decay experiments. All measurements were done in our basement laboratory at Los Alamos National Laboratory. The laboratory building is at an atmospheric depth of 792 g/cm^2 and provides about 1 meter of water equivalent (m.w.e.) concrete (77 g/cm^2) overburden against cosmic-ray muons.

Three data sets were taken with a Canberra Eurysis clover detector [11]. This detector is a set of four n-type, segmented germanium detectors. The four crystals have a total natural germanium mass of 3 kg, and each crystal is segmented in half. The clover detector and its operation in our laboratory were described in Ref. [12]. The remaining two measurements were done with an ORTEC PopTop detector [13] set up in coincidence with a NaI detector. The PopTop is a 71.8-mm long by 64-mm diameter p-type Ge detector. Taking into account the central bore, the detector is 215 cm^3 or 1.14 kg. The NaI crystal is 15.25-cm long by 15.25-cm diameter and is directly connected to a phototube. All data were read out using a pair of XIA LLC's [14] digital gamma finder four-channel (DGF-4C) computer automated measurement and control (CAMAC) modules. The CAMAC crate is connected to the peripheral component interconnect (PCI) bus of a Dell Optiplex computer running Windows 2000. The system was controlled using the standard software supplied by XIA. This data acquisition software runs in the Igor Pro environment [15] and produces binary data files that were read in and analyzed using the ROOT framework [16].

The data sets included (1) a background run with the clover, (2) a Th-wire source run with the clover, (3) an AmBe source run with the clover using two different geometries of moderator, (4) an AmBe source run with the PopTop surrounded by lead, and (5) an AmBe source run with the PopTop surrounded by copper. In this section, we describe the experiments and the data collected.

A. Experimental configurations

The clover was surrounded by 10 cm of lead shielding to reduce the signal from ambient radioactivity. Underneath and above the lead was 5 cm of 30%-loaded borated polyethylene to reduce thermal neutrons. The background run done in this configuration lasted 27.13 days of live time. The configuration for the Th-source run was similar but with some lead removed to expose the detector to the source. The Th-source run had a live time of 1337 s.

The setup was modified somewhat from this background-run configuration for the measurements with the AmBe source. Figure 1 shows the configuration for one of the AmBe measurements. For these data, the clover was shielded on four sides with 10 cm of lead. The AmBe source, 30 mCi of ^{241}Am with a calibrated neutron yield of $\approx$63000 Hz ($\pm$0.7%), was on one side of the clover, with 5 cm of lead and a layer of pure polyethylene moderator (either 10 or 15 cm thick) between the source and detector. The data acquisition system was inactive during data transfer. Only the AmBe runs had a large enough event rate for the dead time to be appreciable. A 6.13-h live-time data run (57% live) was taken with 15 cm of moderator, and another 3.57-h live-time data (38% live) run was taken with 10 cm of moderator (pictured). For the analysis presented below, the data from these two configurations were combined, and thus the AmBe-clover data set contains 9.7 h of live time. The observed energy spectrum extended from $\approx$10 to 3100 keV for these data sets.

During the analysis of the AmBe data, we observed a weak line at 3062 keV. This energy corresponds to a γ-ray transition in ^{207}Pb, and we therefore hypothesized that it was generated via Pb$(n, n'\gamma)$. The double-escape-peak (DEP) energy (2040 keV) associated with this γ ray is very dangerous for ^{76}Ge neutrinoless double-β decay experiments because it falls so close to the transition energy (2039 keV). Furthermore, because the DEP is a single-site energy deposition, it cannot be distinguished from double-β decay through event topology.

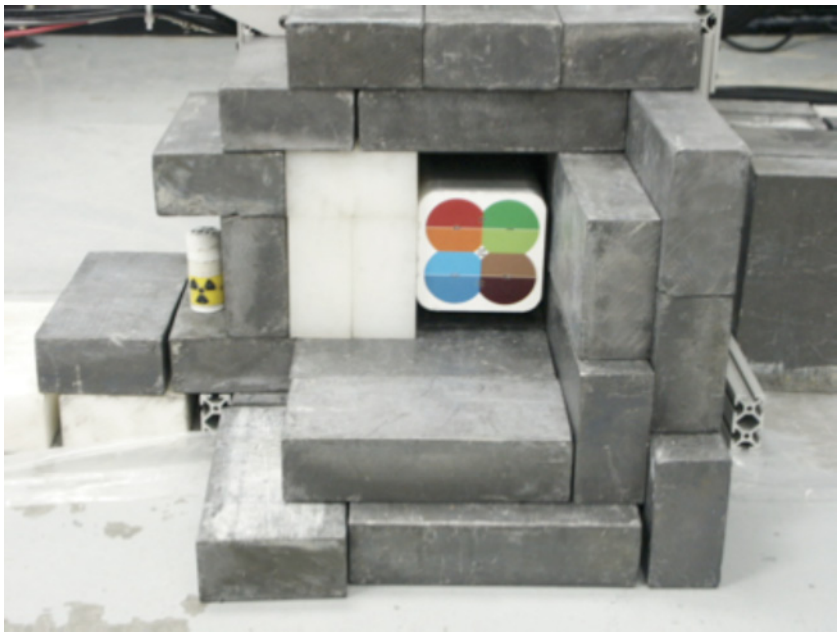

FIG. 1. (Color online) Clover detector as configured for the AmBe source run. The setup at the time of this photograph used 4 in. of polyethylene. One wall of the lead shield was removed only to clarify the relationship between the AmBe source, moderator, and the clover.

This is in contrast to a full-energy γ-ray peak, which tends to consist of several interactions and therefore is a multiple-site deposition. (See Ref. [12] for a discussion of the use of event topology to reduce background in Ge detectors.)

The final two measurements were made with the intention of studying this 3062-keV line in the spectrum and demonstrate its origin. In both cases, a PopTop Ge detector faced a 15.25×15.25 cm NaI detector for coincidence data. By sequentially placing a Pb and then a Cu absorber between an AmBe source and a PopTop Ge detector, we tested the hypothesis that the line was due to neutron interactions in Pb. By looking for a coincident energy deposit in the NaI detector, we could be assured the Ge detector signal originated from a neutron interaction in the sample. An energy deposit threshold in the NaI of greater than 200 keV was required for a coincidence. The PopTop was placed 27.3 cm from the NaI detector with the source placed 20.3 cm (7 cm) from the Ge (NaI) detector. For the lead study, 5 cm of lead was placed directly between the Ge detector and the source. Additional lead, in the form of 5-cm-thick bricks, was positioned around the four sides of the Ge detector to reduce room background. For the copper study, a 0.5-cm thick Cu tube was placed around the PopTop, and a 5-cm Cu block was placed between the PopTop and the source. For this final run, all the lead was removed. For both of these sets of data, the observed spectra extended from ≈125 keV to ≈9 MeV. For the PopTop data, the Pb and Cu runs were 19.12 and 17.76 h of live time, respectively.

B. Data sets

The crystals were individually calibrated, and the resulting spectra summed together to form a single histogram. The peaks within each of the three clover data sets were identified and their intensities determined. If an event had two crystals that responded in coincidence, the histogram would have two entries. Therefore the spectra we analyzed and simulated included all single-crystal energy deposits. By not eliminating events that registered signals in more than one of the clover Ge detectors, we maximized the event rate. The peak strengths were estimated by fitting a Gaussian shape to peaks and a flat background to the spectrum in the region near the peak. For the nuclear recoil lines, the peak shape was assumed to be a triangle and not Gaussian. In Table I, the uncertainties derive from this fit. A summary of the peak strengths is given in Table I, and the spectra themselves are shown in Fig. 2. The data sets were chosen to help decouple line blendings. Because the rates in all peaks and continua are much higher for the source-induced data than for the background, features in those spectra are due to the sources, and other contributions can be safely ignored. For example, the 2614.5-keV line can arise from either the decay of ^{208}Tl or ^{208}Pb$(n, n'\gamma)$. When exposed to a Th source, Tl decay dominates the spectrum, whereas when exposed to an AmBe source, $(n, n'\gamma)$ dominates. Hence by normalizing the rate in this line to the rate in a pure neutron-induced transition [e.g., the 596-keV ^{74}Ge$(n, n'\gamma)$], we can determine the relative contribution of the two processes to the background spectrum. In fact, in the background data, both processes contribute to this line.

TABLE I. Summary of the observed lines in the various spectra taken with the clover detector. Blank entries indicate that no significant peak feature above the continuum was found. Single and double escape peaks are labeled by SEP and DEP, respectively. Line assignments for which we are unsure are indicated by a question mark. Line energies are taken from the *Table of Isotopes* [17].

Energy (keV)	Process	Count rates		
		Backgrnd (per h)	Thorium (Hz)	Clover AmBe (Hz)
23.4	^{70}Ge(n, γ)			1.017(5)
46.5	^{210}Pb	112.75(42)		
53.2	^{234}U	61.01(31)		2.079(8)
53.5	^{72}Ge(n, γ)			
63.2	^{234}Th	93.02(38)		
67.7	^{230}Th	24.05(19)		0.591(4)
68.8	^{72}Ge(n, γ)			0.440(4)
72.80	Pb x-ray		10.5(1)	0.506(4)
74.97	Pb x-ray	663.5(1.0)	34.1(2)	1.703(7)
76.7	Unidentified		29.0(2)	
84.4	^{228}Th	115.28(42)	10.9(1)	0.930(5)
84.5	Pb x-ray			
84.9	Pb x-ray			
87.2				
87.4	Pb x-ray	55.65(29)	16.8(1)	0.262(3)
87.9				
89.9	Th x-ray		32.4(2)	
92.7	^{234}Th	171.38(51)		0.060(1)
93.4	Th x-ray		47.5(2)	
96.0	^{115}In(n, γ)?			0.166(2)
99.5	^{228}Ac	13.71(15)	3.0(1)	
105.3	Unidentified	8.99(12)		
104.8	Th x-ray		20.6(1)	
105.6				
108.7	Th x-ray		7.6(1)	
109.9	^{19}F$(n, n'\gamma)$	43.00(26)		0.506(4)
129.1	^{228}Ac	12.91(14)	3.2(1)	
139.7	^{74}Ge(n, γ)	47.20(27)		2.339(8)
143.9	^{230}Th	20.03(18)		
154.0	^{228}Ac	7.69(11)	1.5(1)	
159.7	^{77}Ge^{m}			0.114(2)
162.4	^{115}In(n, γ)	10.71(13)		1.073(6)
174.9	^{70}Ge(n, γ)	7.45(11)		0.763(5)
186.1	^{226}Ra	114.60(42)		0.323(3)
186.2	^{115}In(n,γ)			
197.1	^{19}F$(n, n'\gamma)$	81.04(35)		2.328(8)
198.4	^{71}Ge sum			
199.2	^{228}Ac		0.66(2)	
202.6	^{115}In(n, γ)			0.061(1)
209.5	^{228}Ac	19.38(17)	10.9(1)	
215.5	^{228}Th	2.43(6)	0.92(3)	
238.6	^{212}Pb	295.77(67)	139.9(1)	0.105(2)
242.0	^{214}Pb	57.49(30)	9.2(1)	
247.1	^{70}Ge(n,γ)			0.070(1)
253.7	^{74}Ge(n,γ)	2.76(7)		0.410(3)
270.2	^{228}Ac	21.39(18)	9.1(1)	

TABLE I. *(Continued.)*

Energy (keV)	Process	Count rates		
		Backgrnd (per h)	Thorium (Hz)	Clover AmBe (Hz)
273.0	^{115}In(n,γ)			0.055(1)
277.4	^{208}Tl ^{208}Pb$(n,n'\gamma)$	12.98(14)	5.4(1)	0.086(2)
284.6	Unidentified	2.79(7)		
288.1	^{212}Bi ?		1.03(3)	
295.2	^{214}Pb	58.02(30)		
297.2 298.7	^{72}Ge(n,γ) ^{115}In(n,γ)			0.068(1)
300.1	^{212}Pb	18.59(17)	9.7(1)	
306.2	^{70}Ge(n,γ)	1.12(4)		0.046(1)
321.4	^{228}Ac		0.67(2)	
326.0	^{70,72}Ge$(n,n'\gamma)$			0.487(4)
328.3	^{228}Ac	10.02(12)	8.2(1)	
332.9	^{228}Ac		1.14(3)	
335.5	^{115}In(n,γ)			0.028(1)
338.7	^{228}Ac	45.13(26)	31.5(2)	
351.9	^{214}Pb	95.11(38)		
354.1	Unidentified			0.043(1)
385.1	^{115}In(n,γ)			0.048(1)
391.3	^{70}Ge(n,γ)			0.053(1)
409.8	^{228}Ac	4.05(8)	4.3(1)	
416.9	^{116}In^{m}	2.21(6)		0.359(3)
438.9	^{40}K DEP	2.54(6)		
445.2	^{74}Ge(n,γ)			0.037(1)
452.3	^{212}Bi?		0.82(2)	
463.3	^{228}Ac	10.96(13)	9.2(1)	
474.0	^{72}Ge(n,γ) ?	2.54(6)		
478.6	^{228}Ac		0.39(2)	
470–485	^{10}B$(n,\alpha)^{7}$Li* ^{7}Li$^{*}(\gamma)^{7}$Li Doppler Broadened			signf.
492.9	^{73}Ge(n,γ)			0.123(2)
499.9	^{70}Ge(n,γ)			0.453(4)
503.9	^{228}Ac		0.34(2)	
509.3 510.7 510.7 510.9	^{228}Ac ^{208}Tl ^{208}Pb$(n,n'\gamma)$ Annih.γ	171.93(51)	16.8(1)	3.409(10)
516.2	^{35}Cl(n,γ)			0.160(2)
537.5	^{206}Pb$(n,n'\gamma)$	5.12(9)		0.158(2)
562.9 563.0	^{228}Ac ^{76}Ge$(n,n'\gamma)$	12.83(14)	1.52(3)	0.244(3)
569.7	^{207}Pb$(n,n'\gamma)$	14.17(15)		0.422(4)
572.3	^{228}Ac		0.53(2)	
574.7	^{74}Ge(n,γ)			0.091(2)
583.1	^{208}Tl ^{208}Pb$(n,n'\gamma)$	71.64(33)	49.6(2)	0.256(3)
595.9	^{74}Ge$(n,n'\gamma)$ ^{73}Ge(n,γ)	59.90(30)		1.869(7)
608.3	^{73}Ge(n,γ)			0.333(3)

TABLE I. *(Continued.)*

Energy (keV)	Process	Count rates		
		Backgrnd (per h)	Thorium (Hz)	Clover AmBe (Hz)
609.2	^{214}Bi	60.11(30)		
629.6	^{72}Ge$(n,n'\gamma)$			0.078(2)
648.2	^{115}In(n,γ)			0.025(1)
657.2	^{206}Pb$(n,n'\gamma)$			0.047(1)
662.0	^{137}Cs	9.04(12)		
663.8	^{206}Pb$(n,n'\gamma)$			0.069(1)
669.0	^{70}Ge$(n,n'\gamma)$			0.030(1)
692.4	^{72}Ge$(n,n'e^{-})$	87.70(37)		2.406(8)
701.0	^{74}Ge$(n,n'\gamma)$			0.082(2)
708.2	^{70}Ge(n,γ)			0.176(2)
727.3	^{212}Bi	15.72(16)	11.7(1)	
747.7	^{70}Ge(n,γ)			0.047(1)
755.3	^{228}Ac	2.19(6)	1.52(3)	
763.1	^{208}Tl		0.85(3)	
763.1	^{208}Pb$(n,n'\gamma)$?			0.032(1)
766.6 768.4	^{224m}Pa ^{214}Bi	4.85(9)		
771.8	^{228}Ac	2.02(6)	2.11(4)	
782.0	^{228}Ac		0.67(2)	
785.5	^{212}Bi	4.19(8)	1.57(3)	
786.3 786.8	^{35}Cl(n,γ) ^{208}Pb$(n,n'\gamma)$			0.041(1)
788.4 788.7	^{35}Cl(n,γ) ^{70}Ge(n,γ)			0.064(1)
795.0	^{228}Ac	7.92(11)	6.1(1)	
798.0	^{208}Pb$(n,n'\gamma)$			0.023(1)
803.1	^{206}Pb$(n,n'\gamma)$	20.90(18)		0.850(5)
806.2	^{214}Bi	3.03(7)		
808.2	^{70}Ge(n,γ)			0.048(1)
818.6	^{116}In^{m}			0.064(1)
824.9		1.03(4)		
830.4	^{228}Ac		0.70(2)	
834.1	^{72}Ge$(n,n'\gamma)$	45.15(26)		0.290(3)
835.6	^{228}Ac		2.30(4)	
840.4	^{228}Ac		1.19(3)	
843.8	^{27}Al$(n,n'\gamma)$	4.48(8)		0.112(2)
846.9	^{76}Ge$(n,n'\gamma)$			0.062(1)
860.4 860.4	^{208}Tl ^{208}Pb$(n,n'\gamma)$	8.64(12)	6.0(1)	0.090(2)
865.0	Unidentified			0.094(2)
867.9	^{73}Ge(n,γ)	4.25(8)		0.466(4)
881.0	^{206}Pb$(n,n'\gamma)$	2.50(6)		0.151(2)
892.9	^{212}Bi		0.42(2)	
894.3	^{72}Ge$(n,n'\gamma)$			0.029(1)
897.8	^{207}Pb$(n,n'\gamma)$	6.28(10)		0.199(2)
904.1	^{228}Ac		0.94(3)	
911.2	^{228}Ac	48.86(27)	37.1(2)	
934.1	^{214}Bi	1.99(6)		
958.4	^{228}Ac		0.37(2)	
960.9	^{74}Ge$(n,n'\gamma)$			0.095(2)
964.4	^{228}Ac	11.22(13)	6.2(1)	
968.8	^{228}Ac	26.83(20)	21.6(1)	
981.0	^{206,8}Pb$(n,n'\gamma)$			0.035(1)

TABLE I. *(Continued.)*

Energy (keV)	Process	Count rates		
		Backgrnd (per h)	Thorium (Hz)	Clover AmBe (Hz)
988.4	^{228}Ac	1.95(5)	0.20(1)	
993.7	^{74}Ge$(n,n'\gamma)$			0.026(1)
995.1	^{206}Pb$(n,n'\gamma)$			
999.5	^{74}Ge$(n,n'\gamma)$			0.034(1)
1001.5	^{224}Pa^{m}	8.03(11)		
1004.5	^{228}Ac		0.17(1)	
1014.5	^{27}Al$(n,n'\gamma)$	7.46(11)		0.173(2)
1033.1	^{228}Ac		0.20(1)	
1040.1	^{70}Ge$(n,n'\gamma)$	16.89(16)		0.210(2)
1040.8				
1063.7	^{207}Pb$(n,n'\gamma)$	8.47(11)		0.145(2)
1065.0	^{228}Ac		0.47(2)	
1078.8	^{212}Bi	1.11(4)	0.62(2)	
1093.9	^{208}Tl sum		0.90(3)	
	511+583			
1095	^{207}Pb$(n,n'\gamma)$			
1095.8	^{70}Ge(n,γ)	7.81(11)		0.464(4)
1096.9	^{116m}In			
1101.3	^{74}Ge$(n,n'\gamma)$			0.123(2)
1105.6	^{74}Ge$(n,n'\gamma)$			0.019(1)
1110.4	^{228}Ac sum		0.52(2)	
1120.6	^{214}Bi	11.70(13)		
1122.5	^{228}Ac sum		0.26(1)	
1126	^{208}Pb$(n,n'\gamma)$			0.022(1)
	^{72}Ge$(n,n'\gamma)$			
1131.6	^{73}Ge(n,γ)?	1.34(5)		0.034(1)
1139.4	^{70}Ge(n,γ)	1.34(5)		0.077(2)
1153.5	^{228}Ac		0.15(1)	
1155.2	^{214}Bi	1.08(4)		
1164.9	^{35}Cl$(n,n'\gamma)$	0.49(3)		0.072(1)
1166.0	^{72}Ge$(n,n'\gamma)$			
1173.5	^{60}Co	13.67(14)		
1201.2	$p(n,\gamma)d$			0.415(3)
	DEP			
1204.2	^{73}Ge(n,γ)	9.39(12)		0.163(2)
	^{74}Ge$(n,n'\gamma)$			
1226.7	^{74}Ge$(n,n'\gamma)$			0.017(1)
1238.4	^{214}Bi	5.22(9)		
1246.9	^{228}Ac		0.58(2)	
1261.0	^{74}Ge$(n,n'\gamma)$			0.019(1)
1281.0	^{214}Bi	0.74(3)		
1286-7	^{228}Ac Blend		0.14(1)	
1293.5	^{116}In^{m}	4.09(8)		0.462(4)
1298.8	^{70}Ge(n,γ)			0.087(2)
1332.5	^{74}Ge(n,n'γ)			0.018(1)
1332.5	^{60}Co	12.27(14)		
1344.5	^{74}Ge(n,γ)			
1345.9	^{206}Pb$(n,n'\gamma)$	0.52(3)		0.017(1)
1347.7	^{70}Ge(n,γ)			
1374.2	^{228}Ac sum		0.28(1)	
	964 + 409			
	911 + 463			

TABLE I. *(Continued.)*

Energy (keV)	Process	Count rates		
		Backgrnd (per h)	Thorium (Hz)	Clover AmBe (Hz)
1378.0	^{214}Bi	3.24(7)		
1378.8	^{70}Ge(n,γ)			0.065(1)
1393.8	^{206}Pb$(n,n'\gamma)$			0.016(1)
1401.5	^{214}Bi	0.58(3)		
1408.6	^{214}Bi	1.84(5)		
1413.6	^{73}Ge$(n,n'\gamma)$			0.018(1)
1431.1	^{228}Ac		0.15(1)	
1433.5	^{206}Pb$(n,n'\gamma)$			0.020(1)
1436.9	^{208}Pb$(n,n'\gamma)$			0.017(1)
1459.2	^{228}Ac		0.80(2)	
1461.0	^{40}K	30.18(22)		0.066(1)
1463.9	^{72}Ge$(n,n'\gamma)$			0.114(2)
1466.8	^{206}Pb$(n,n'\gamma)$			0.032(1)
1471.6	^{73}Ge(n,γ)			0.047(1)
1489.2	^{74}Ge$(n,n'\gamma)$			0.025(1)
1496.2	^{228}Ac	0.73(3)	0.85(3)	
1501.7	^{228}Ac		0.42(2)	
1508.9	^{116}In^{m}			0.069(1)
1508.9	^{214}Bi	1.95(3)		
1512.7	^{212}Bi		0.38(2)	
1538	^{214}Bi	0.54(3)		
1557.1	^{228}Ac		0.14(1)	
1580.8	^{228}Ac	0.68(3)	0.55(2)	
1588.3	^{228}Ac	6.06(10)	2.94(5)	
1592.5	^{208}Tl DEP			
1592.5	^{208}Pb DEP	7.24(11)	2.10(4)	0.107(2)
1593.0	^{207}Pb$(n,n'\gamma)$			
1599.3	^{214}Bi	0.38(2)		
1601.1	^{35}Cl(n,γ)			0.018(1)
1602.0	^{74}Ge$(n,n'\gamma)$			
1614.9	^{208}Pb$(n,n'\gamma)$?			0.020(1)
1620.5	^{212}Bi	1.81(5)	1.32(3)	
1625.0	^{228}Ac		0.34(2)	
1630.7	^{228}Ac	1.82(5)	1.46(3)	
1631.5	^{74}Ge$(n,n'\gamma)\gamma)$			0.021(1)
1632.0	^{70}Ge(n,γ)			
1634.0	^{76}Ge(n,γ)			0.016(1)
1638.3	^{228}Ac	0.43(3)	0.41(2)	
1640.4	^{208}Pb$(n,n'\gamma)$			0.026(1)
1640	^{74,76}Ge$(n,n'\gamma)$			
1661.3	^{214}Bi	0.36(2)		
1666.3	^{228}Ac		0.17(1)	
1699.5	^{206}Pb$(n,n'\gamma)$?			0.021(1)
1704.5	^{206}Pb$(n,n'\gamma)$	0.72(3)		0.041(1)
1710.9	^{72}Ge$(n,n'\gamma)$			0.327(3)
1712.2	$p(n,\gamma)d$ SEP			0.156(2)
1725.7	^{207}Pb$(n,n'\gamma)$			0.029(1)
1729.6	^{214}Bi	3.59(7)		
1764.7	^{214}Bi	11.68(13)		
1779.0	^{27}Al(n,γ)^{28}Al	2.13(6)		0.127(2)
	^{28}Al $\Rightarrow$ ^{28}Si			
1806.0	^{212}Bi		0.11(1)	

TABLE I. *(Continued.)*

Energy (keV)	Process	Count rates		
		Backgrnd (per h)	Thorium (Hz)	Clover AmBe (Hz)
1844.5	^{206}Pb$(n,n'\gamma)$			0.044(1)
1846.9	^{214}Bi	2.26(6)		
1940.4	^{74}Ge$(n,n'\gamma)$			0.027(1)
1951.1	^{35}Cl(n,γ)			0.032(1)
1959.3	^{35}Cl(n,γ)			0.023(1)
2092.1 2092.7	^{206}Pb$(n,n'\gamma)$ ^{207}Pb$(n,n'\gamma)$			0.039(1)
2103.8	^{208}Tl SEP ^{208}Pb SEP	5.21(9)	2.25(4)	0.090(2)
2112.1	^{116m}In			0.061(1)
2118.5	^{214}Bi	0.64(3)		
2204.0	^{214}Bi	3.73(8)		
2223.3	$p(n,\gamma)d$			5.813(13)
2390.5	^{116}In^{m}			0.015(1)
2448.5	^{214}Bi	0.51(3)		
2614.5	^{208}Tl ^{208}Pb$(n,n'\gamma)$	39.39(25)	16.3(1)	0.729(5)
2650.3	^{206}Pb$(n,n'\gamma)$?			0.011(1)
2686	sum ^{208}Tl?		0.12(1)	
2892	sum ^{208}Tl		0.08(1)	
3061.9	^{207}Pb$(n,n'\gamma)$			0.010(1)

Some comments on our choices for line identification are in order. For an isotope such as ^{72}Ge, where a neutron capture leads to a stable nucleus, almost all (n,γ) lines could also be interpreted as $(n,n'\gamma)$ lines in the resulting nucleus; in this case, ^{73}Ge. For isotopes within the detector, however, such as the 53.5-keV ^{72}Ge(n,γ) transition, the competing ^{73}Ge$(n,n'\gamma)$ line would be a sum of this γ-ray energy and the recoil nucleus energy. At these low energies, where the recoil is a fair fraction of the γ-ray energy, the $(n,n'\gamma)$ would simply contribute to the continuum and not be observed as a line. For the high-energy cases, the blend of a monoenergetic γ-ray line and a $(n,n'\gamma)$ process might be present.

For the calibration runs, our threshold was approximately 70 keV. Also note that we used a thorium wire as a calibration source. Since the wire is pure natural Th, we observe the Th x rays in that data. In contrast, the background run shows lines from the thorium chain as a contaminant; therefore those lines are absent.

In all spectra, there are a few lines we have not identified.

C. Neutron spectra simulation

Fast neutrons (from 100 MeV to 1 GeV or more) tend to produce additional neutrons through nuclear reactions as they traverse high-Z material. In particular, the flux of neutrons will increase several-fold while the average neutron energy decreases through these processes. As a result, fast neutrons will penetrate deep into a shield producing additional neutrons at lower energies. These low-energy neutrons ($\lesssim$20 MeV) give rise to a substantial γ-ray flux, because $(n,n'\gamma)$ cross sections are large near 10 MeV but become small at higher energies. Hence it is these secondary lower energy neutrons that interact with the shield and detector materials to produce γ rays, which can give rise to background in double-β decay experiments. To understand the process by which high-energy neutrons influence the low-energy neutron flux and, in turn, the observed γ-ray flux, we simulated neutrons impinging on an outer shield and tracked how their spectrum changed as the particles traversed the shield. We also simulated the production of neutron-induced γ rays and how the Ge detector responded to them. Specifically, we performed simulations of several geometries:

(i) A simulation of the cosmic-ray produced neutrons with energy up to 1 GeV at our laboratory in Los Alamos and their propagation through a 10-cm Pb shield and the response of the clover detector to γ rays produced by neutron interactions in the shield. This simulation, compared against our background data, tests the precision to which we can model neutron production, scattering with secondary neutron production, and $(n,n'\gamma)$ interactions.

(ii) A simulation of the neutron flux induced on the clover from the AmBe source (neutron energy $\leqslant$11.2 MeV) passing through 15 cm of polyethylene before impinging on the 10-cm Pb shield. Since the neutron flux is of low energy, this simulation tests the precision to which we model $(n,n'\gamma)$ interactions.

(iii) A simulation of the neutron flux with neutron energies up to a few GeV expected at 3200 m.w.e. deep due to cosmic-ray μ interactions in the surrounding rock and 30-cm lead shield and the resulting response of the clover to the flux of γ rays arising from this flux. This simulation permits us to estimate rates in detectors situated in underground laboratories.

The purpose of the first two simulations is to verify the code's predictive power. The third is to aid in understanding the utility of depth to avoid neutron-induced backgrounds.

The simulation package GEANT3-GCALOR [18,19] is described in detail in Ref. [10]. In general, (n,n') reactions leave the target nucleus in a highly excited state which subsequently decays via a γ-ray cascade to the ground state. In the simulation, inelastic scattering cross sections for excitation to a given level depends on the properties of the ground and excited states. These cross sections were calculated using in-house-written code based on Hauser-Feshbach [20] theory modified by Moldauer [21]. The validation of the Hauser-Feshbach theory has been the subject of several studies [22–24]. The simulated γ-ray flux arises from the relaxation of the initial excited-state distribution, which includes a large number of levels [60 states for ^{208}Pb$(n,n'\gamma)$ reactions, for example]. The nuclear levels and their decay channels were provided by the ENSDF [25] database through the GEANT package. Note, however, that the simulation did not predict every possible transition. In particular, the important 2041- and 3062-keV emissions from Pb were not part of this simulation. This situation arises because the simulation packages only have (n,n') cross sections for the lowest lying excited states for most nuclei. It is set to zero for most other levels. The

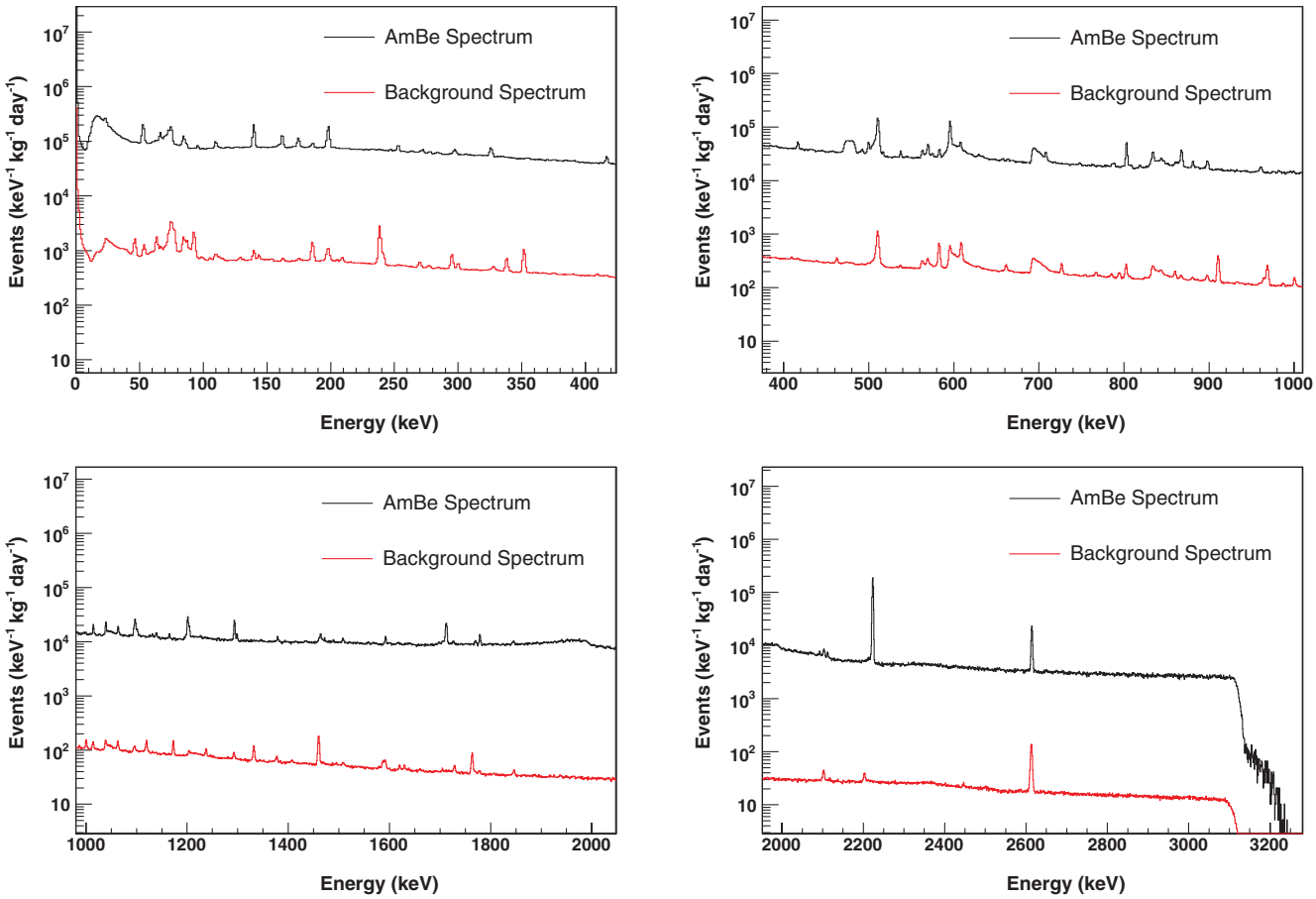

FIG. 2. (Color online) AmBe and background spectra taken with the clover detector.

details of this simulation are described in Ref. [10]. Here we study the effectiveness of the simulation to predict spectra resulting from $(n, n'\gamma)$.

The simulation was done by generating neutrons with the appropriate energy spectrum outside the lead shield and propagating them through the shield including secondary interactions that may add to the neutron flux and alter the energy spectrum. Figure 3 shows a comparison between the data and the simulations for the clover background run and AmBe run. Note only neutrons as primary particles were simulated for this comparison, and the dominant difference between the two spectra is due to the room's natural radioactivity and non-neutron μ-induced processes. Here we excluded those processes from the simulation to emphasize the spectral shape, including lines that are a direct result of neutron interactions. The similarity of the spectra in Fig. 3 indicates that the measured background spectrum is dominated by neutron-induced reactions.

The uncertainty in the simulation is calculated by comparing the well-known peaks in Table II, which compares the simulation results with the line production for both background and AmBe runs. The measured neutron-produced lines are within about 5% of the predicted values from simulation, as is the continuum rate in the AmBe data. Therefore the $(n, n'\gamma)$ rates are well simulated for nuclear states with well-defined cross sections. (The continuum for the background data includes processes that were not simulated and hence is not a good measure of the uncertainty.) Because the neutron flux estimates come from these line strengths (See Sec. III), the uncertainty in the flux cancels in these estimates. The uncertainty in the measured neutron flux and spectrum underground (≈35%) constrains the precision to which such simulations can be verified and is well described in Ref. [10]. This 35% uncertainty due to the flux is much larger than the uncertainty for the γ-ray line production described above. Therefore, a total uncertainty of 35% is used for all predictions of line rates underground throughout this paper.

III. NEUTRON FLUX

In this section, we use the data to determine the neutron fluxes we observed during our various experimental configurations. We then compare our measured cosmic-ray induced flux with that predicted from past measurements and our simulation.

A. Ge$(n, n'\gamma)$ analysis

Spectral lines that indicate neutron interactions in natural Ge detectors have been studied previously; see Refs. [26–29], for example. In particular, the sawtooth-shaped peaks due

TABLE II. Comparison of the simulated to measured rates (background: per hour and AmBe: Hz) for several lines produced by neutron interactions. The 2041- and 3062-keV lines are not included in the simulation.

Process	γ-ray energy (keV)	Background-clover Simulation	Background-clover Measurement
^{74}Ge$(n,n'\gamma)$	596	56.21	59.90(30)
^{74}Ge$(n,n'\gamma)$	254	2.63	2.76(7)
^{76}Ge$(n,n'\gamma)$	2023	3.2×10^{-7}	below sensitivity
^{206}Pb$(n,n'\gamma)$	537	4.82	5.12(9)
^{207}Pb$(n,n'\gamma)$	898	6.21	6.28(10)
^{206}Pb$(n,n'\gamma)$	1706	0.69	0.72(3)
^{206}Pb$(n,n'\gamma)$	2041	none	not seen
Continuum region	2000–2100	110.2	187.35(19)
^{207}Pb$(n,n'\gamma)$	3062	none	not seen
		AmBe-clover	
^{74}Ge$(n,n'\gamma)$	596	1.8	1.87
^{74}Ge$(n,n'\gamma)$	254	0.36	0.41
^{76}Ge$(n,n'\gamma)$	2023	8.5×10^{-4}	below sensitivity
^{206}Pb$(n,n'\gamma)$	537	0.15	0.16
^{207}Pb$(n,n'\gamma)$	898	0.14	0.20
^{206}Pb$(n,n'\gamma)$	1706	0.04	0.04
^{206}Pb$(n,n'\gamma)$	2041	none	not seen
Continuum region	2000–2100	7.01	7.33
^{207}Pb$(n,n'\gamma)$	3062	none	0.01

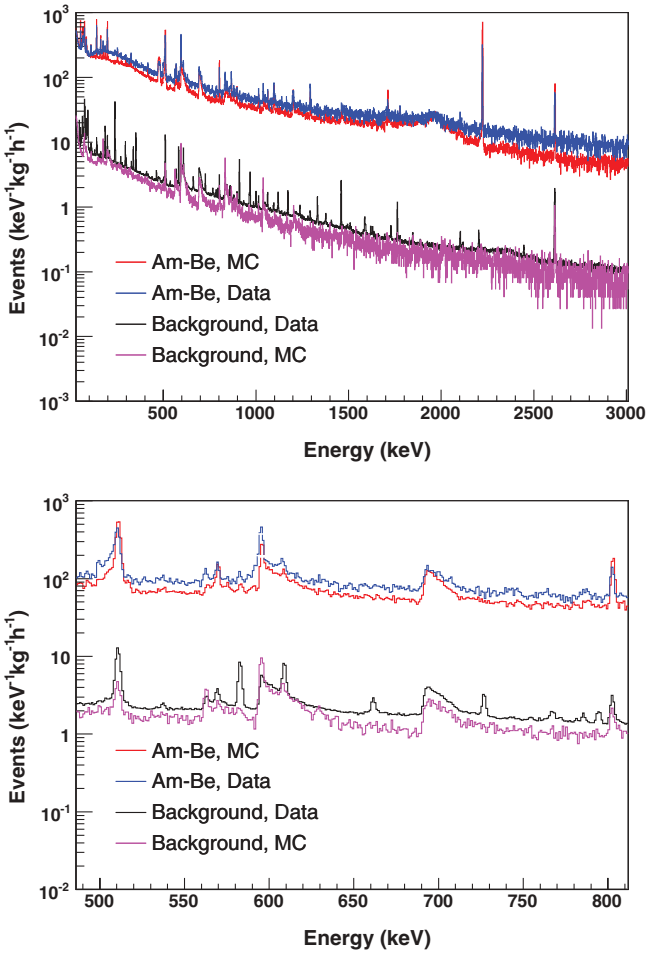

FIG. 3. (Color online) Comparison of the measured and simulated AmBe spectra for the clover detector surrounded by 10 cm lead and 15 cm of moderator. The upper plot shows the energy range between 10 and 3100 keV. The lower plot shows the range 470–830 keV where the most significant $(n,n'\gamma)$ lines can be seen. The simulated AmBe neutron spectrum was normalized to the AmBe source strength for 6.13-h live-time. The measured total neutron flux in the background spectrum (see Sec. III C) was used to normalize the simulated background spectrum. Note, only neutrons as primary particles were simulated for this comparison, and the difference between the spectra is due to the room's natural radioactivity and non-neutron, μ-induced processes.

to ^{72,74}Ge(n,n') at 693 and 596 keV, respectively, are clear indications of neutrons and have been used to deduce neutron fluxes [30]. By operating Ge detectors in a low-background configuration, these lines can be used to help interpret the background components. Recent double-β decay experiments [5,6] used detectors constructed from Ge enriched in isotope 76. Although an appreciable amount of ^{74}Ge remained (14%), ^{70,72,73}Ge were depleted. For such detectors, only lines originating in isotopes 74 and 76 are useful for neutron interaction analysis. As these experiments reach for lower backgrounds, neutron-induced backgrounds become a greater concern, and the diagnostic tools more important.

Neutrons from (α,n) and fission reactions have an energy spectrum with an average energy similar to the AmBe spectrum used in this study. Furthermore, the average energy of the AmBe neutrons is similar to that of the neutrons within the hadronic cosmic-ray flux impinging on our surface laboratory, although the latter extend to much higher energies. Therefore the Ge-detector signatures indicating the presence of neutrons described above will be similar to those arising from neutrons originating from the rock walls of an underground laboratory. However, low-background experiments that use Ge detectors are typically deep underground and shielded from environmental radioactivity by a thick shield. This shield, typically made of Pb, is then usually surrounded by a neutron moderator. This configuration is effective at greatly reducing the neutron flux originating from (α,n) and fission reactions in the cavity walls of the underground laboratory. In contrast, although neutrons originating from μ interactions underground are much more rare, they have much higher energy. Therefore these μ-induced neutrons can penetrate the shield more readily and become a major fraction of the neutrons impinging on the detector.

B. AmBe neutron flux

The estimate of the flux of neutrons with energies greater than 692 keV is given as [30–32]

$$\Phi_n = k\frac{I}{V}, \tag{1}$$

where I is the counts s^{-1} under the asymmetric 692-keV peak, V is the volume of the detector in cm^3 (566 cm^3), and k is a parameter found by Ref. [30] to be 900 ± 150 cm. For the 15-cm moderator data, this formula predicts a neutron flux of $2.3/cm^2$ s; whereas our simulation, using the known flux of the source, predicts $1.8/cm^2$ s. This difference (20–30%) is somewhat greater than the 17% uncertainty claimed by Ref. [30]. The geometry for our measurement was complicated, and perhaps this added complexity of neutron propagation contributes to the difference. For the uncertainty associated with the flux of neutrons produced from cosmic ray μ, we use the 35% value, as it is much larger than the value associated with Eq. (1).

For the AmBe neutron source, the rate in the 692-keV peak is 2.406 ± 0.008 Hz. This results in $\Phi_n^{\mathrm{AmBe}} = 3.8 \pm 1.1/cm^2$ s. This rate is an average over the two moderator configurations. The neutron flux during the 10-cm moderator run is estimated to be about a factor of 2.3 larger than for the 15-cm moderator run. For the PopTop-AmBe run on Pb for the raw data (in coincidence with the NaI detector), the effective flux was $8.6 \pm 2.6/cm^2$ s ($0.26 \pm 0.08/cm^2$ s).

C. Cosmic-ray induced neutron fluxes

In the background spectrum, the rate in the 692-keV peak is 87.7 ± 0.4/h. Using Eq. (1) with $I = (2.44 \pm 0.06) \times 10^{-2}$ Hz for the background spectrum, one obtains a fast neutron flux of $\Phi_n^{\mathrm{back}} = (3.9 \pm 1.2) \times 10^{-2}/cm^2$ s at the detector in our surface laboratory.

Reference [30] provides a similar formula to estimate the thermal neutron flux, which is accurate to approximately 30%. Using the intensity of the 139.68-keV γ-ray line of ^{75m}Ge, it is

$$\Phi_{\mathrm{th}}\left(\frac{n}{\mathrm{cm^2\ s}}\right) = \frac{980 I_{139.68}}{\left(\epsilon^{\gamma}_{139.68} + 1.6\right) V}, \tag{2}$$

with

$$\epsilon^{\gamma}_{139.68} \simeq 1 - \frac{1 - e^{-V^{1/3}}}{V^{1/3}}, \tag{3}$$

where $I = 47.2 \pm 0.3/\mathrm{h} = 0.013$ Hz is the event rate in the peak of the 139.68-keV line, and V is the volume of the detector in cm^3. Using $V = 566\ cm^3$, we obtain $\Phi_{\mathrm{th}}^{\mathrm{back}} = (9.1 \pm 2.7) \times 10^{-3}/cm^2$ s. We also measure the thermal neutron flux for the AmBe neutron source, $\Phi_{\mathrm{th}}^{\mathrm{AmBe}} = 1.6 \pm 0.5/cm^2$ s.

Thus the total neutron flux incident on the Ge detector measured for the background run is approximately $\Phi_{\mathrm{tot}}^{\mathrm{back}} = \Phi_n^{\mathrm{back}} + \Phi_{\mathrm{th}}^{\mathrm{back}} = (4.8 \pm 0.7) \times 10^{-2}/cm^2$ s.

D. Neutron flux as a function of depth

In our basement laboratory, there are three primary sources of environmental neutrons. The largest contribution comes from the hadronic cosmic-ray flux. The next largest arises from μ interactions in the 77 g/cm^2 thick overhead concrete layer in the building. Finally, there is the negligible contribution from (α, n) and fission neutrons from natural radioactivity in the room. The atmospheric depth at the altitude of our laboratory is 792 g/cm^2. Including the concrete, the depth is 869 g/cm^2. Using the analysis of Ziegler [33,34], the flux at our laboratory due to the hadronic flux can be estimated to be 3.0 times larger than that at sea level. The flux at sea level has been measured to be $1.22 \times 10^{-2}/cm^2$ s [35] resulting in a flux in our laboratory of $3.7 \times 10^{-2}/cm^2$ s. To estimate the additional neutron flux originating from μ interactions in the concrete above our laboratory, we rely on our simulations of neutron generation and propagation. The simulation predicts $1.4 \times 10^{-2}/cm^2$ s ($3.3 \times 10^{-2}/cm^2$ s) for the muon-induced (hadronic) neutron flux inside the lead shield for a total simulated neutron flux of $4.7 \times 10^{-2}/cm^2$ s in acceptable agreement with our measurement of $(4.8 \pm 2.2) \times 10^{-2}/cm^2$ s = $(1.51 \pm 0.69) \times 10^6/cm^2$ yr. The success of this simulation lends credence to the neutron flux estimate in the following sections.

The neutron flux onto the detector will be increased as a result of the neutron interactions with shield materials and neutron back-scattering from the cavity walls. For example, our simulations show that the fast neutron flux will increase by a factor of $\approx$10 by traversing a 30-cm lead layer. Also, neutrons will backscatter from the cavity walls and reflect back toward the experimental apparatus, effectively increasing the impinging neutron flux by a factor of 2–3 depending on the specific geometries of the detector and experimental hall. Therefore, it is important to account for these effects when estimating the neutron flux at the detector.

Muon-induced neutron production in different shielding materials and in the detector itself was also studied in Ref. [10]. For example, with 30 cm of lead surrounding a clover-style detector at 3200 m.w.e., the total muon-induced neutron flux impinging on the detector was calculated to be $(8.6 \pm 4.0) \times 10^{-8}/cm^2 s = 2.7 \pm 1.2/cm^2$ yr. Some of the interactions resulting from these neutrons would be eliminated by a μ veto. Assuming a veto efficiency of 90% for muons traversing this lead shield, the effective neutron flux is estimated to be $(2.0 \pm 0.9) \times 10^{-8}/cm^2$ s = $0.63 \pm 0.29/cm^2$ yr. The energy spectrum of neutrons at the lead/detector boundary at 3200 m.w.e. is shown in Fig. 4 and has an average value of 45 MeV.

The average energy of the μ-induced neutrons is 100–200 MeV and much higher than that of (α, n) neutrons ($\approx$5 MeV). The simulated flux of the μ-induced neutrons $[(2 \pm 0.9) \times 10^{-8}/cm^2 s = 0.63 \pm 0.29/cm^2$ yr] inside the detector shield at a depth of 3200 m.w.e. is a factor of 2.4 greater than the simulated (α, n) flux surviving the shield $[(0.85 \pm 0.39) \times 10^{-8}/cm^2 s = 0.27 \pm 0.12/cm^2$ yr]. The average energy of these (α, n) originating neutrons is 3–5 MeV at the detector surface.

With this estimate of the neutron flux at depth and with our measurements of the Pb and Ge neutron-induced detector response, we can proceed to estimate these processes in underground Ge-detector experiments. There are effects in addition to the incident flux, however, that must be taken into account when extrapolating our surface laboratory results to different geometries and locations.

(i) As the thickness of the Pb shield increases, additional secondary neutrons will be generated. Our simulation

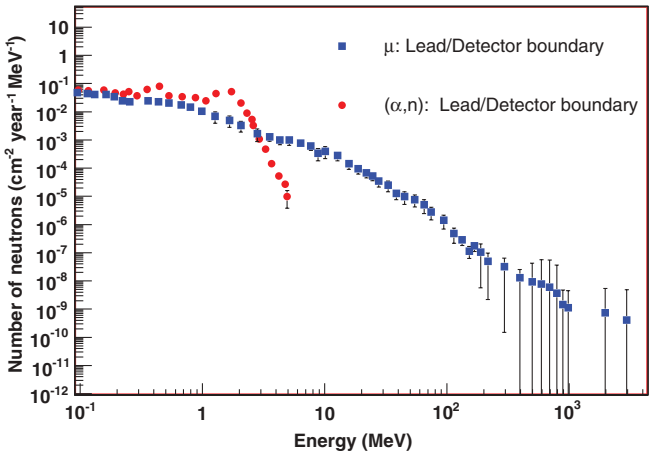

FIG. 4. (Color online) Effective neutron flux onto the simulated detector described in the text at a depth of 3200 m.w.e. Shown are the neutron fluxes from two sources: (1) the effective neutron flux induced by muons that transverse the surrounding rock and shielding materials assuming a 90% muon-veto efficiency and (2) the neutron flux from (α, n) reactions in the rock.

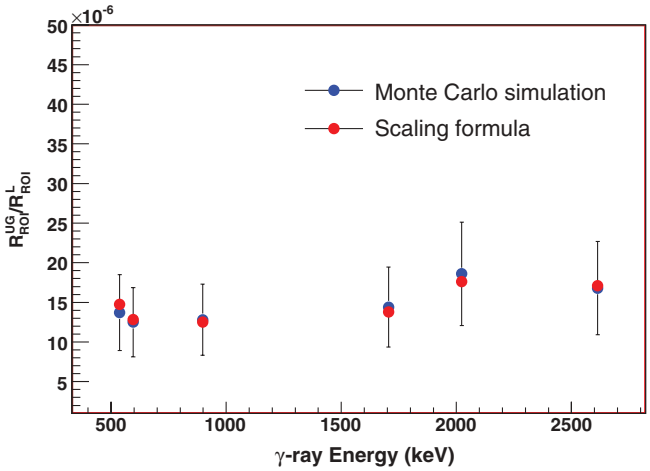

FIG. 5. (Color online) Comparison between the Monte Carlo simulation of a detector as described in the text and the scaling formula for several excitation lines. The 35% uncertainties arise from the cross-section uncertainty and the statistical uncertainty of determining the peak counts in the simulated spectra; the latter dominates.

predicts that a factor of $k_{\text{shield}} = 2.16$ more neutrons will be produced by a 30-cm-thick shield than by a 10-cm-thick shield.

(ii) As the energy of the neutrons increases, the number of multiply scattered neutrons increases, and therefore the number of interactions that might produce a γ ray increases. For the average energy of neutrons at our surface laboratory (at 3200 m.w.e.), the average scattering length is $\lambda_L = 7.1$ cm ($\lambda_{\text{UG}} = 12.5$ cm).

(iii) Also as the energy increases, the number of states that can be excited in the target nucleus increases. In the shield at our surface laboratory (at 3200 m.w.e), the average neutron energy is 6.5 MeV (45 MeV).

All of these factors can be incorporated into a scaling formula derived from our simulation. The rate ($R^{\text{UG}}_{\text{ROI}}$) of background near the region of interest (ROI) in an underground laboratory (UG) can be related to that measured in our surface laboratory (R^{L}_{ROI}) as

$$R^{\text{UG}}_{\text{ROI}} = \left(1 + \frac{\lambda_{\text{UG}}}{\lambda_L}\right) k_{\text{shield}} \left[\left(\frac{E^{\text{UG}}_n - E_x}{E^{L}_n - E_x}\right)^{0.8}\right] \frac{\Phi^{\text{UG}}_n}{\Phi^{L}_n} R^{L}_{\text{ROI}}, \tag{4}$$

where Φ^{L}_n (Φ^{UG}_n) is the neutron flux in our surface laboratory (at 3200 m.w.e.), E_n is the neutron energy, and E_x is the excitation energy for a typical level. This formula reproduces our simulated results well, and the uncertainty of its use is dominated by the precision of the simulation. Using the 2.6-MeV level in ^{208}Pb as an example, $R^{\text{UG}}_{\text{ROI}} \sim 1.7 \times 10^{-5} R^{L}_{\text{ROI}}$. Figure 5 shows a comparison between the Monte Carlo simulation and the scaling formula Eq. (4) for several lines.

IV. ANALYSIS

A. Pb($n, n'\gamma$) analysis

If fast neutrons are present, then one will also see γ-ray lines from Pb(n, n') interactions. In very low background configurations, γ rays from neutron-induced excitations in ^{208}Pb and ^{207}Pb can be masked by or confused for decays of ^{208}Tl and ^{207}Bi, respectively. Therefore it is the stronger transitions in ^{206}Pb (537.5, 1704.5 keV) that are most useful for determining if these processes are taking place. In ^{207}Pb, the relative strength of the 898-keV transition, compared to the 570- and 1064-keV transitions, is much stronger when it originates from ^{207}Pb$(n, n'\gamma)$ as opposed to ^{207}Bi β decay to ^{207}Pb. Therefore this line can also be used as a tell-tale signature of neutron interactions.

Our data show indications of ^{206,207,208}Pb$(n, n'\gamma)$. As noted earlier, the 2614-keV γ ray from ^{208}Pb can originate from ^{208}Tl decay or from ^{208}Pb$(n, n'\gamma)$. The 692-keV peak arises only from neutron interactions on ^{72}Ge. Since the Pb shielding was similar in both the background and AmBe runs, we can compare the ratio of the rate in the 2614-keV peak with that in the ^{72}Ge$(n, n'\gamma)$ 692-keV peak in the two data sets to deduce the fraction of the 2614-keV in the background run that can be attributed to neutron interactions. This ratio in the AmBe spectrum is 0.30, and that in the background spectrum is 0.45; therefore, we conclude that ≈67% of the strength in the background run is due to neutron reactions and the remainder is due to ^{208}Tl decay. Clearly, in our surface laboratory, environmental neutrons are a significant contributor to the observed signal.

B. Special cases of the 2023-, 2041-, and 3062-keV γ rays

The 2023-keV level in ^{76}Ge can be excited by neutrons. The simulation predicts that this line is too weak to be seen

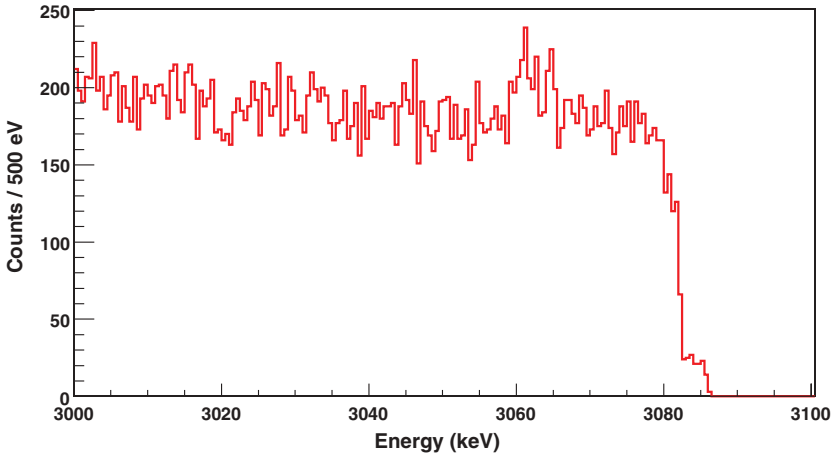

FIG. 6. (Color online) Energy spectrum near 3000 keV showing the ^{207}Pb$(n, n'\gamma)$ 3062-keV γ-ray line in the AmBe spectrum with the clover detector.

in the clover AmBe data, but the clover is built of natural Ge. In the enriched detectors planned for future double-β decay experiments, the fraction of isotope 76 is much larger, and this line would be enhanced. Still, our simulation (Table V) predicts it would be a very small peak.

The 3714-keV level in ^{206}Pb can emit a 2041-keV γ ray. We only observed a candidate γ-ray peak in the coincidence data (Ge detector event in coincidence with a 4.4-MeV γ ray in the NaI detector) with the AmBe source radiating the Pb shield around the PopTop detector. The magnitude of this peak, if it exists, is small and not convincing. We use this data set to place a limit on the production rate of this line, as it results in the most conservative limit.

In the AmBe-irradiated clover and the noncoincidence PopTop spectra, we observed a 3062-keV γ ray that we assign to a transition from the 3633-keV level in ^{207}Pb (see Fig. 6). This line is only present when Pb surrounds the detector; it is absent when Cu forms the shield. The statistical sensitivity was too weak in the PopTop coincidence spectrum to observe this weak line. In the clover AmBe spectrum, the rate of this line is 5.3×10^{-3} times that of the 596-keV ^{74}Ge peak rate; and in the raw AmBe PopTop with Pb spectrum, the ratio is 4.5×10^{-3}. From these data, we can estimate an approximate rate that these dangerous backgrounds would be produced for a given neutron flux. In our surface laboratory, the clover background rate for the ^{74}Ge 596-keV peak was 59.9 events/h. This leads to a predicted rate of 0.3 events/h in the 3062-keV peak. Note that our data indicate that any peak at 3062 keV is statistically weak ($\leqslant$0.2 events/h) but reasonably consistent with this prediction. Note, in the AmBe-clover runs, polyethylene blocks were used to increase the flux of thermal neutrons. It appears that these blocks contain some Cl, and therefore we see indications of Cl(n, γ) lines. Even though ^{35}Cl has a neutron capture line at 3062 keV, we do not assign the observed line in our data to that process. Because the ^{35}Cl(n, γ) line at 2863 keV is not observed and because the line at 1959 keV is weak, we conclude that assigning this line to Cl would be inconsistent with the predicted line ratios for neutron capture. However, a concern regarding our assignment of the 3062-keV line to ^{207}Pb is that one also expects a 2737-keV emission from the same 3633-keV level. This companion γ ray is not observed in our data, and we plan future measurements dedicated to measuring the neutron-induced relative intensities of these two lines. If we assume that the entire rate (0.01 Hz) of the 3062-keV line is due to $(n, n'\gamma)$, we can make a crude estimate of the cross section by scaling to the rate in the 2614-keV line. The cross section for the 2614-keV $(n, n'\gamma)$ is 2.1 b $\pm$ 10% [23]. Using this cross section, the relative rates in the two peaks, the different isotopic ratios of ^{208}Pb and ^{207}Pb, and the different γ-ray detection efficiencies, the average cross section for ^{207}Pb(4.5-MeV (n, n') 3062-keV γ ray) is estimated to be 75 mb. The uncertainty is estimated to be about 20% or $\sim$15 mb.

From measurements with the clover and a ^{56}Co source, which has γ-ray energies near 3100 keV, we expect 0.13 DEP events per full-energy γ-ray event. Therefore, in our surface laboratory, we expect 0.03 events/h in the DEP at 2039 keV due to ^{207}Pb$(n, n'\gamma)$. This is well below our continuum rate of 2.5 events/keV h or 10/h in an energy window corresponding to a 4-keV wide peak.

Since our simulation does not predict all these lines, we summarize the measured rates normalized to the neutron flux in Table III to provide simple scaling to different experimental configurations. The uncertainties in Table III are estimates based on a minor contribution of the statistical uncertainty in the peak strengths and a major contribution resulting from the $\approx$35% uncertainty in the neutron flux determination as described in Sec. III B. Because the uncertainty is mostly systematic, there is a good possibility that the total uncertainties for each individual measurement are correlated. Therefore, to estimate the average values in this table, we took a straight average of the individual values and then assigned an uncertainty equal to the largest fractional value. This procedure, although not rigorous, is more conservative than a weighted average. In addition, some peaks were not observed in all spectra. The upper limits on the strength of these peaks were estimated from the rates of weakest peaks observed near the associated energy region in the spectrum. Such peaks are considered to represent the level of sensitivity of our peak detection procedures. The 2041-keV line is a special case. We quote an upper limit based on the only spectrum that indicated a possible peak.

These measurements were done for a clover detector inside a 10-cm Pb shield. The relative energy-dependent efficiency

TABLE III. Raw count rates for select processes normalized to neutron flux of 1/cm^2 yr. When extrapolating to neutron energies distant from that near the measurements, the uncertainty (35%) associated with the extrapolation must be included. See text for a discussion of the uncertainty estimates in this table especially with respect to the average.

Process	Rate (events/ton yr)			
	AmBe-clover	AmBe-PopTop	Background	Average
^{206}Pb$(n, n'537\text{-keV}\gamma)$	13.9 ± 4.9	20.5 ± 7.2	12.2 ± 4.3	15.5 ± 5.4
^{74}Ge$(n, n'596\text{-keV}\gamma)$	164 ± 57	unresolved[a]	142 ± 50	153 ± 54
^{207}Pb$(n, n'898\text{-keV}\gamma)$	17.5 ± 6.1	21.2 ± 7.4	14.9 ± 5.2	17.9 ± 6.3
^{206}Pb$(n, n'1705\text{-keV}\gamma)$	3.6 ± 1.3	3.2 ± 1.1	1.7 ± 0.6	2.8 ± 1.0
^{206}Pb$(n, n'2041\text{-keV}\gamma)$	<6.3	<0.5	<1.7	<5.0[b]
^{207}Pb$(n, n'3062\text{-keV}\gamma)$	0.88 ± 0.31	0.6 ± 0.21	<1.0	0.7 ± 0.2
Continuum rate[c] from Pb,Ge$(n, n'\gamma)$	2.6 ± 0.9	2.0 ± 0.7	2.5 ± 0.9	2.4 ± 0.8

[a]In the PopTop data, the 596-keV line was not resolved from nearby lines.
[b]The 2041 line was not observed in any of our spectra; however, a weak peaklike feature was present in the AmBe-PopTop coincidence data. We used the upper limit for the rate in that peak as the "average," because we considered that to be most conservative.
[c]Events/keV ton yr.

ϵ_{rel} for a full-energy peak in the clover can be approximated by

$$\epsilon_{\text{rel}} = 0.15 + 0.93 \exp \frac{-(E_\gamma - 148)}{766}, \tag{5}$$

where E_γ is the γ-ray energy in keV. This expression is normalized to 1.0 at 209 keV and is estimated to have an accuracy of about 20% near 200 keV, which improves to about 10% at 2600 keV. The quoted relative efficiency for each of the four individual clover detectors is 26% at 1.33 MeV as quoted by the manufacturer. Table III does *not* incorporate this efficiency correction; therefore, the table presents the measured count rates with a minimum of assumptions. The thickness of Pb is large compared to the mean free path of the γ rays of interest; therefore, the scaling should hold for other thick-shield configurations. Even so, the rates will be geometry dependent, so these results can only be considered as guides when applied to other experimental designs. The rate of these excitations also depends on neutron energy. For the background run (AmBe run) the average neutron energy is ≈6.5 MeV (≈5.5 MeV). Our simulations predict that the rate of these excitations scales as energy to the 0.81 power.

V. DISCUSSION

A. Model of the clover background

We can use these experimental results to create a background model for our surface laboratory and deduce the contribution to the continuum near 2039 keV due to $(n, n'\gamma)$ reactions. We then use simulation of high-energy neutron production and propagation to extrapolate this model to better understand experiments done at depth. The measured rate for the continuum near 2039 keV was 14.8 events/keV kg d. For the Th-wire data, this continuum rate was 0.10 events/keV s (2900 events/keV kg d) and for the AmBe data it was 0.09 events/keV s (2600 events/keV kg d). To determine the neutron-induced continuum rates in the AmBe data, however, we have to correct for the contribution from the tail of two high-energy γ rays that are not part of the neutron-induced spectrum in the background. These are the γ rays from the 2223-keV $p(n, \gamma)d$ and the 4.4-MeV γ rays originating from the (α, n) reaction of the AmBe source itself. Although only ≈10% of these AmBe γ rays penetrate the 5-cm Pb shield, there is still a significant flux.

A simple simulation of the detector response to 2223-keV γ rays can easily determine the ratio of the rate in the 2039-keV region to that in the full-energy peak. Simulation indicates that this ratio is 5.2×10^{-2}/keV. Since the full-energy peak count rate is 5.813 Hz, we find this contribution to the continuum is 0.03 events/keV s. For the 4.4-MeV γ ray from the source itself, simulation must determine an absolute rate in the continuum, because the high-energy threshold prevents the observation of the full-energy peak or its escape peaks. The simulation predicts 0.03 events/keV s. Subtracting these two contributions from the continuum rate for the AmBe source near 2039 keV results in a final value of 0.03 events/keV s or 860 events/keV kg d.

Our background measurements were done without a cosmic-ray anticoincidence system. From auxiliary measurements with a scintillator in coincidence with the clover detector and a similar shielding geometry, we measured the rate of μ passing through the detector. In the continuum near the 2039-keV region, the rate is 5.4 events/keV kg d.

From the Th-wire source data, we measure the ratio of the rate in the continuum near 2039 keV to that in the 2614 keV (16.3 Hz) peak to be 6×10^{-3}/keV. Of the 2614-keV peak rate in the background data, ≈33% is due to ^{208}Tl decay. Scaling from the 2614-keV peak in the background data, the count rate near the 2039-keV region due to the Compton tail of the ^{208}Tl 2614-keV peak is 0.7 events/keV kg d.

TABLE IV. Summary of the count rate in the clover-detector background data in the energy region near 2039 keV based on the model deduced for the surface laboratory described in the text. The precision of the neutron-induced and muon-induced spectra simulations (Sec. II C and Ref. [10]) is estimated to be about 35%. We take this to be a conservative estimate for the uncertainties associated with this table.

Process	Clover event rate Surface lab (events/keV kg d)
Neutron-induced	8.3 ± 2.9
^{208}Tl Compton scattering	0.7 ± 0.3
High-energy μ continuum	5.4 ± 1.9
Total from model	14.4 ± 5.0
Measured rate	14.8 ± 0.2

The remainder of the 2614-keV peak is due to neutron-induced processes. The contribution due to neutrons can be estimated from the AmBe data. For the AmBe data, the ratio of the rate in the continuum near the 2039-keV region (0.03 events/keV s) to that for the 596-keV ^{74}Ge$(n, n'\gamma)$ peak (1.87 Hz) is 1.6×10^{-2}/keV. Scaling from the ^{74}Ge peak rate in the background data (59.9/h) indicates a rate of 7.8 events/keV kg d in the continuum near 2039 keV. That is, 53% of the events in that region are due to neutrons. One can do a similar scaling from the 692-keV ^{72}Ge rates. Here the ratio is 1.3×10^{-2}/keV and the continuum rate is 8.8 events/keV kg d. We use the average of the Ge values as our estimate (8.3 events/keV kg d = 3030 events/keV kg yr) for the neutron-induced contribution to the continuum rate. Table IV summarizes the deduced contributions to the spectrum in the 2039-keV region in the clover background spectrum, and the following section discusses how these data are used along with simulation to estimate rates in experimental apparatus underground.

B. Solving the problem with overburden

The primary purpose of this study is to better understand the impact of neutrons on the background for future double-β decay experiments. In this subsection, we use neutron fluxes from our simulations of the surface laboratory, measurements with the AmBe source, and simulations of the neutron flux in an underground laboratory to estimate the contribution of neutron-induced backgrounds underground. In the following subsection, we examine data from previous underground experiments.

The simulation of neutron processes in the 10-cm Pb shield and Ge comprising the clover detector at the altitude of our laboratory predicts about 1594 ± 558 events/keV kg yr between 2000 and 2100 keV due to lead excitation and about 1337 ± 468 events/keV kg yr in this energy region due to germanium excitation. Our measured value for the neutron-induced events is 3030 ± 1061 events/keV kg yr to be compared with this predicted value of 2931 ± 1026 events/keV kg yr.

The simulation of the clover within a 30-cm lead shield at a depth of 3200 m.w.e. predicts about 0.019 ± 0.007 events/keV kg yr contributed by lead excitation and about 0.016 ± 0.006 events/keV kg yr contributed by germanium excitation for a total of 0.035 ± 0.012 events/keV kg yr. One can also just scale our surface-laboratory measurement of the neutron-induced rate near 2039 keV by the factor derived from Eq. (4) above. This results in 0.05 ± 0.02 events/keV kg yr. For a detector like the clover, analysis based on pulse shape discrimination (PSD) and the response of individual segments or crystals can help reduce background based on its multiple-site energy deposit nature. These backgrounds can then be distinguished from the single-site energy deposit character of double-β decay. We have measured the background reduction factor via these techniques to be $\approx$5.9 for the clover detector [12].

Reference [10] provides a "quick reference" formula for estimating the neutron flux as a function of depth. The μ flux and its associated activity is reduced by $\approx$10 for every 1500 m.w.e of added depth. Future double-β decay experiments hope to reach backgrounds near 0.25 events/keV ton yr. Our estimate of the rate at 3200 m.w.e. is 35-50 events/keV ton yr, which is a factor of 150 above the goal. Hence, greater depths would be desirable.

C. Discussion of previous underground experiments

Previous Ge-based double-β decay experiments conducted deep underground [5,6] set the standard for low levels of background. The future proposals [8,9], however, hope to build experiments with much lower backgrounds. In this subsection, we estimate how large the neutron contribution was to the previous efforts and may be to future designs. Using the scaling summarized in Eq. (4), we can compare the expectations of our simulated underground apparatus with previously published results. Table V shows this comparison. This table also presents a summary of how the rates would be affected by a change in depth only. The IGEX Collaboration [5] has not published its data in sufficient detail to do a similar comparison. Other underground Ge detector experiments do not have the required sensitivity.

The Heidelberg-Moscow experiment [6] is a critical case study for such backgrounds, and it was operated at a depth of 3200 m.w.e. One is clearly led to consider if the 3062-keV γ ray can explain the signal reported in Refs. [36,37]. Figure 36 in Ref. [36] shows that no more than a few counts can be assigned to a 3062-keV γ ray. If the 23 counts assigned to double-β decay were actually a DEP from this γ ray, then one would expect 175 counts or so in the 3062-keV peak. Therefore, it is difficult to explain the claimed peak by this mechanism. It is also clear that the predicted rate of the 2041-keV γ ray is too low to explain their data. The data from Ref. [36] show lines at 570 and 1064 keV, and the authors assigned these lines to ^{207}Bi present in the Cu. However, the spectra displayed in Fig. 13 of that paper shows that only detectors surrounded by Pb indicate the 570-keV line. Since there is no evidence for the 898-keV line in the data, we

TABLE V. Summary of key count rates (events/ton yr) arising from neutron interactions in the clover background data in the energy region near 2039 keV as predicted by our analysis for three representative depths. The shield thickness is taken to be 30 cm, and a veto system with an assumed efficiency of 90% is included. Except for the 2023-keV line, we used the scaling of Eq. (4) to scale our clover background measurements to the 3200 m.w.e. depth and then used the muon fluxes at WIPP, Gran Sasso, and SNOLAB [10] to scale to the other depths. The Ge rates are also scaled for an enriched detector (86% isotope 76, 14% isotope 74). The scalings require the results from the simulations. The uncertainty is dominated by the simulated flux uncertainty and is estimated to be 35%. Since we did not observe the 2023-keV line, we used simulation to predict the rate. We used the measured upper limit for the 2041-keV line. For comparison, the results of Ref. [36] are shown. Reference [36] claims a result for zero-neutrino double-β decay in an experiment performed at 3200 m.w.e. We entered the claimed event rate for that process in the same row as the 2041-keV line for comparison. The rate limits for the other lines assigned to Ref. [36] result from our estimates based on the figures in that reference and does not come directly from that work.

Process	1600 m.w.e.	3200 m.w.e.	6000 m.w.e.	Ref. [36]
^{74}Ge 596 keV	19400 ± 6800	1130 ± 400	15 ± 5	<800
^{76}Ge 2023 keV	30 ± 10	2 ± 1	0.02 ± 0.01	300
^{206}Pb 537 keV	4400 ± 1500	250 ± 88	3.4 ± 1.2	
^{207}Pb 898 keV	5300 ± 1900	310 ± 110	4.2 ± 1.5	
^{206}Pb 1705 keV	610 ± 210	36 ± 13	0.5 ± 0.2	
^{206}Pb 2041 keV	$<1300 \pm 450$	$<74 \pm 26$	$<1.0 \pm 0.3$	400
^{207}Pb 3062 keV	145 ± 51	8.4 ± 2.9	0.1 ± 0.03	<71
Continuum[a]	880 ± 310	50 ± 17	0.7 ± 0.24	110

[a]Events/keV ton yr.

agree with the ^{207}Bi assignment; however, we hypothesize that it must reside in the Pb and not the Cu. Perhaps this contamination is cosmogenically produced in Pb when it resides on the surface and not as a result of bomb testing as hypothesized by the authors [36].

Reference [36] also observed lines at 2011, 2017, 2022, and 2053 keV. These lines had rates of approximately 500, 500, 300, and 380 events/ton yr, respectively. The line at 2022 keV is near a line we predict at 2023 keV. Reference [36] attributes these lines to weak transitions in ^{214}Bi. Our analysis indicates that a negligible fraction of the peak at 2023 keV is neutron induced. However, since the predicted strength of the tell-tale lines that would indicate a presence of neutron interactions is just below the sensitivity of that experiment, this conclusion is not without uncertainty. It has been pointed out that the strength in the 2022-keV line is too strong with respect to the ^{214}Bi branching ratios even when summing uncertainties are taken into account [38,39]. The analysis in Ref. [38], however, was based on an incorrectly normalized Fig. 1 in Ref. [6]. A recent analysis [39] taking this into account still points to an inconsistency in the line strengths. This discrepancy could be resolved if one attributes a significant fraction of that peak to neutron interactions on ^{76}Ge. Such an attribution is not supported by our simulations.

Reference [37] simulates the background in the Heidelberg-Moscow experiment resulting in a predicted signal of 646 ± 93 counts in the region between 2000 and 2100 keV during an exposure of 49.6 kg yr. This is a count rate of 130/keV ton yr to be compared with the quoted measured value for the data period simulated of 160/keV ton yr. Their estimate indicates that only 0.2/keV ton yr are due to neutrons, and they argue that μ-generated neutrons are a negligible contribution. Our estimates indicate that neutrons are a more significant contribution and that the μ contribution is significant. We are aware of no direct neutron flux measurements for neutrons above 25 MeV. The flux of neutrons with energy greater than 25 MeV is estimated in Ref. [37] to be 10^{-11}/cm^2 s and they considered these neutrons to produce a negligible contribution to the background. In contrast, the simulation in Ref. [10] gives 56×10^{-11}/cm^2 s at 3200 m.w.e for the neutrons with energy greater than 25 MeV. We use this higher flux value, and as a result, our estimate of the background rate near 2 MeV of 50/keV ton yr is comparable to the excess (30/keV ton yr) of the measured rate in comparison to the simulated rate in Ref. [37].

D. Is copper an alternative to lead?

One has to consider the existence of a DEP line at the double-β decay endpoint a serious design consideration for Ge-detector experiments. From the above analysis, the dangerous lines at 2041 and 3062 keV due to Pb$(n, n'\gamma)$ are not significant contributors to the spectrum of Ref. [36]. However, as future efforts reduce the natural activity irradiating the detectors, these Pb-neutron interactions will become important. One solution could be the use of Cu as a shield instead of Pb. Copper is rather expensive, and building the

entire shield of this material is probably not necessary. A thick inner liner of Cu might suffice, but if a peak is observed and Pb is present near the detector, arguments based on the spectrum near 3062 keV will be critical.

Although the problematic lines we observed in the Pb data were absent in our Cu data, the shields were too dissimilar to make a quantitative comparison regarding the effectiveness of reducing the continuum background. Furthermore, our experience with lead and the simulation of $(n, n'\gamma)$ spectra reduces confidence in the conclusion regarding Cu in the absence of such data. We are preparing better experimental studies to address this question.

VI. CONCLUSION

As double-β decay experiments become more sensitive, the potential background must be constrained to ever lower levels. Much progress has been made in reducing naturally occurring radioactive isotopes from materials from which the detector is constructed. As these isotopes that have traditionally limited the experimental sensitivity are eliminated, rarer processes will become the dominant contributors. Here we have considered neutron-induced processes and have quantified them. Reactions involving neutrons can result in a wide variety of contributions to the background. That is, no single component is likely to dominate. Therefore, tell-tale signatures for neutrons are needed and were identified in this work.

In addition to the general continuum background that neutrons might produce, two specific dangerous Pb$(n, n'\gamma)$ lines were identified. These two backgrounds can be significantly reduced using depth and/or an inner layer of Cu within the shield. In particular, the 3062-keV transition in ^{207}Pb has a double escape peak at the endpoint energy for double-β decay in ^{76}Ge. A comparison of past double-β decay data indicates the rate of this transition is too small to explain a claim of double-β decay.

ACKNOWLEDGMENTS

We thank R. L. Brodzinski for discussions regarding the historical production of ^{207}Bi and its possible presence in the environment. We thank John Wilkerson and Jason Detwiler for useful suggestions and discussion. Finally, we also thank Alan Poon and Werner Tornow for useful discussions and a careful reading of the manuscript. This work was supported in part by Laboratory-Directed Research and Development at Los Alamos National Laboratory.

[1] Steve R. Elliott and Petr Vogel, Annu. Rev. Nucl. Part. Sci. **52** 115 (2002).
[2] Steven R. Elliott and Jonathan Engel, J. Phys. G: Nucl. Part. Phys. **30**, R183 (2004).
[3] F. T. Avignone III, G. S. King III, and Yuri Zdesenko, New J. Phys. **7**, 6 (2005).
[4] A. S. Barabash, Phys. At. Nucl. **67**, No. 3, 438 (2004).
[5] C. E. Aalseth *et al*., Phys. Rev. C **59**, 2108 (1999).
[6] H. V. Klapdor-Kleingrothaus *et al*., Eur. Phys. J. A **12**, 147 (2001).
[7] H. V. Klapdor-Kleingrothaus *et al*., Nucl. Instrum. Methods Phys. **522**, 371 (2004).
[8] R. Gaitskell *et al.* (Majorana Collaboration), arXiv:nucl-ex/0311013.
[9] I. Abt *et al*., arXiv:hep-ex/0404039.
[10] D.-M. Mei and A. Hime, Phys. Rev. D **73**, 053004 (2006).
[11] The clover detector used was manufactured by Canberra Eurysis, 800 Research Parkway, Meriden CT 06450, USA.
[12] S. R. Elliott *et al*., Nucl. Instrum. Methods A **558**, 504 (2006).
[13] The PopTop detector is manufactured by ORTEC, 801 South Illinois Ave., Oak Ridge, TN 37830.
[14] XIA LLC, 8450 Central Ave., Newark CA 94560, USA.
[15] Wavemetrics Inc., PO Box 2088, Lake Oswego, OR 97035, USA.
[16] Rene Brun and Fons Rademakers, Nucl. Instrum. Methods **389**, 81 (1997); http://root.cern.ch.
[17] *Table of Isotopes*, edited by Richard B. Firestone and Virginia S. Shirley (Wiley, New York, 1996).
[18] R. Brun *et al*., "GEANT3," CERN DD/EE/84-1 (revised), 1987.
[19] C. Zeitnitz *et al*., Nucl. Instrum. Methods A **349**, 106 (1994).
[20] W. Hauser and H. Feshbach, Phys. Rev. **87**, 366 (1952).
[21] P. A. Moldauer, Phys. Rev. **123**, 968 (1961).
[22] Richard M. Lindstrom *et al*., Nucl. Instrum. Methods A **299**, 425 (1990).
[23] H. Vonach, A. Pavlik, M. B. Chadwick, R. C. Haight, R. O. Nelson, S. A. Wender, and P. G. Young, Phys. Rev. C **50**, 1952 (1994).
[24] A. Pavlik, H. Hitzenberger-Schauer, H. Vonach, A. Pavlik, M. B. Chadwick, R. C. Haight, R. O. Nelson, and P. G. Young, Phys. Rev. C **57**, 2416 (1998).
[25] National Nuclear Data Center, Brookhaven National Laboratory, Upton, NY, 11973-5000.
[26] K. C. Chung *et al*., Phys. Rev. C **2**, 139 (1970).
[27] R. L. Bunting and J. J. Kraushaar, Nucl. Instrum. Methods **118**, 565 (1974).
[28] Richard M. Lindstrom *et al*., Nucl. Instrum. Methods A **299**, 425 (1990).
[29] G. Fehrenbacher, R. Meckbach, and H. G. Paretzke, Nucl. Instrum. Methods A **372**, 239 (1996).
[30] G. P. Škoro *et al*., Nucl. Instrum. Methods A **316**, 333 (1992).
[31] P. H. Stelson *et al*. Nucl. Instrum. Methods A **98**, 481 (1972).
[32] R. Wordel *et al*., Nucl. Instrum. Methods A **369**, 557 (1996).
[33] J. F. Ziegler, IBM J. Res. Dev. **40**, 19 (1996).
[34] J. F. Ziegler, IBM J. Res. Dev. **42**, 117 (1998).
[35] P. Goldhagen *et al*., Nucl. Instrum. Methods **476**, 42 (2002).
[36] H. V. Klapdor-Kleingrothaus, A. Dietz, I. V. Krivosheina, and O. Chkvorets, Nucl. Instrum. Methods A **522**, 371 (2004).
[37] C. Dörr and H. V. Klapdor-Kleingrothaus, Nucl. Instrum. Methods A **513**, 596 (2003).
[38] C. E. Aalseth *et al*., Mod. Phys. Lett. A **17**, 1475 (2002).
[39] R. L. Brodzinski, PNNL-SA-49010, 2006 (unpublished).